Available online at www.sciencedirect.com
ScienceDirect
Ceramics International 35 (2009) 3153–3159
CERAMICS INTERNATIONAL
www.elsevier.com/locate/ceramint

Aqueous tape casting and crystallization behavior of gadolinium-doped ceria

Yen-Pei Fu [a,*], Yen-Chun Liu [b], Shao-Hua Hu [c]

[a] Department of Materials Science and Engineering, National Dong-Hwa University, Shou-Feng, Hualien 974, Taiwan
[b] Department of Graduate School of Optomechatronic and Materials, Wu-Feng Institute of Technology, Ming-Hsiung, Chiayi 621, Taiwan
[c] Department of Environmental Resources Management, Dahan Institute of Technology, Sincheng, Hualien 971, Taiwan

Received 18 March 2009; received in revised form 5 April 2009; accepted 3 May 2009
Available online 6 June 2009

Abstract

An aqueous tape casting of gadolinia-doped ceria (GDC) ceramics was developed using Poly(acrylic acid) PAA as dispersant, Poly(vinyl alcohol) PVA as binder, Poly(ethylene glycol) PEG as plasticizer, and deionized water as solvent. Surface properties of GDC powder with and without PAA dispersant were characterized by electrokinetic measurements. The zeta potential measurement revealed that the isoelectric point for GDC powders in the absence of dispersant corresponds to a pH value of 4.06. The experimental results showed that pH value greatly affects the rheology of the slurry. Homogeneous, smooth, and defect-free green tapes were successfully obtained by using an appropriate slurry formula. Moreover, the crystallization kinetics of GDC powders prepared by coprecipitation process also has been investigated in this study. The activation energy of crystallization was calculated by differential scanning calorimetry (DSC) at different heating rates. Analysis of non-isothermal DSC data presented values of 105.3 kJ/mol and 1.171 for the activation energy of crystallization presented and the Avrami exponent, respectively.

Keywords: A. Powder: chemical preparation; A. Tape casting; C. Thermal properties; D. CeO_2; E. Fuel cells

1. Introduction

Solid oxide fuel cells (SOFCs) are attracting widespread attention due to their high-energy conversion efficiency and low pollution. High oxide ionic conducting solid electrolytes based on zirconia have been intensively investigated [1]. In order to reduce the operation temperature from 1000 to 800 °C or even lower, doped ceria has been considered as the solid electrolyte for moderate temperature solid oxide fuel cells [2]. In contrast to pure zirconia, $CeO_{2-\delta}$ has the fluorite structure with oxygen vacancies ($V_O^{\bullet\bullet}$) as the predominant ionic defects. The oxygen vacancy concentration and concomitant oxide ion conductivity, in CeO_2 can be increased by the substitution of a lower-valent metal such as Y [3], Sm [4,5], Gd [6,7], and Ca [8]. Pure CeO_2 stoichiometric ceramics are a poor oxide ion conductors. However, the ion conductivity can be improved by increasing the oxygen vacancies by the substitution of gadolinium, which is lower than 4+ in valence and upon substituting for Ce^{4+} are charge compensated by oxygen vacancies, for example:

$$Gd_2O_3 \xrightarrow{CeO_2} 2Gd'_{Ce} + 3O_O^x + V_O^{\bullet\bullet}$$

In general, decreasing the thickness of the electrolyte can further reduce the resistance to ionic transport and allows lower operating temperature of SOFCs [9]. Tape casting is mainly used to manufacture thin flat ceramic sheets. The thickness of tape cast products is typically 20 μm to a few millimeters. Typical applications include transducers, capacitors, pyroelectric infrared detectors and SOFCs [10]. Accordingly, in this study, we use tape casting to produce the electrolyte film of GDC for SOFCs.

Traditionally, tape casting was done using organic solvents. Because of environmental, health, safety, and economic reasons, aqueous media substituting organic solvents [11]. Although, aqueous tape casting presented above-mentioned advantages, there are still several problems to overcome such as higher crack sensitivity, slow drying of the tape, flocculation and poor wetting of the slips [12,13]. The stability and

* Corresponding author. Tel.: +886 3 863 4209; fax: +886 3 863 4200.
E-mail address: d887503@alumni.nthu.edu.tw (Y.-P. Fu).

0272-8842/$36.00
doi:10.1016/j.ceramint.2009.05.002

rheological properties of ceramic suspension are influenced by many factors, such as pH, type and amount of dispersant and, the number of active groups on the powder surface. The stability and rheological properties of nanosized ceramics powders are more complex due to the particle interactions [14,15]. In this study, the rheological behavior of the slurries with addition of dispersant, binder, and plasticizer is investigated. Moreover, we also used coprecipitation process to produce GDC powder and studied its crystallization kinetics.

2. Experimental procedures

2.1. Starting materials

$Ce_{0.8}Gd_{0.2}O_{1.9}$ (GDC) was synthesized by a coprecipitation method. Stoichiometric amounts of cerium nitrate hexahydrate ($Ce(NO_3)_3{\cdot}6H_2O$), and gadolinium nitrate hexahydrate ($Gd(NO_3)_3{\cdot}6H_2O$) were dissolved in distilled water and then the ammonia (NH_4OH) solution was added to nitrates solution. Precipitates were obtained until pH = 9.5 for mixed solution. The final concentration of the stock solution was 0.2 M for Ce^{3+}. The resulting precipitate was vacuum-filtered, washed three times with water and ethanol, respectively. Then, precipitate was dried at 80 °C in an oven. The coprecipitated hydrate powder decomposed to a polycrystalline oxide by heating to 600 °C for 2 h. The oxidation of Ce^{3+} to Ce^{4+} occurred during this stage. Deionized water was used as solvent. Poly(acrylic acid) (PAA) with molecular weight of (5000 g/mol) was used as an electrosteric dispersant. Poly(-ethylene glycol) (PEG) with molecular weight of (400 g/mol) was used as plasticizer. Poly(vinyl alcohol) (PVA) with molecular weight of (13 000–18 000 g/mol) was used as binder. All organic additives are soluble in deionized water. The content of organic components in this study was expressed in weight percent with respect to the GDC powder.

2.2. Differential scanning calorimetry measurements

Differential scanning calorimetry (DSC; Model TG-DTA/DSC Setaram, Caluire, France) was used to study the crystallization characterization of coprecipitated GDC powder. A heating rate of 10–25 °C/min was used in DSC measurements up to 600 °C in air. Thermal analysis is done under flowing air at 100 ml/min. An initial sample weight of 12.0 ± 0.2 mg was used in all measurements. In this study, DSC instrument was calibrated using metallic Sn. The melting temperature and latent heat of transformation for Sn are 231.8 °C and 60.46 J/g, respectively. The peak area values and onset temperatures were determined by a test run. These values were inputted and calculated by the software. It automatically revealed the correction data. We can use this correction data to correct our future data collected by the instrument.

2.3. Zeta potential measurements

The zeta potential of suspension was measured using a Malvern Zetasizer nano-series. The suspensions were prepared by dispersing GDC powders (0.01 vol%) in deionized water. The pH value of suspension was adjusted by adding HNO_3 (0.1 M) or NH_4OH (1 M). The suspensions were mixed ultrasonically before the test to ensure that only the mobility of single particle was measured.

2.4. Rheological characteristic of slurry

Viscosity measurements were at room temperature performed using a rotary viscometer (BROOKFIELD DV-II$^+$ Pro viscometer). GDC suspensions were prepared at solid loadings of 55 wt% with 2 wt% of PAA for a dispersant study.

2.5. Slurry preparation and tape casting

The tape cast slurries were prepared in two stages. First, GDC powder and deionized water with optimum content of dispersant were mixed in a polyethylene jar with ZrO_2 balls for 18 h. Next, the binder and plasticizer solution were milled for 18 h to obtain good homogeneity. Subsequently, the slurry was vacuumed to deair. The optimum composition of slurry is given in Table 1. Tape casting was achieved using a laboratory-sale with a moving casting head on mylar substrate film. The tape casting machine (Eph Engineering Associates, Inc., Orem, UT, USA) has a moving blade on a glass slab. After tape casting, the tapes were left to dry at room temperature. In this study, a casting speed of 20 mm/s and a blade gap height of 0.30 mm were chosen. The green tape thicknesses were in the range of 150–200 μm.

2.6. Characterization techniques

A computer-interfaced X-ray powder diffractometer (XRD) with Cu K_α radiation (λ = 1.5418 Å) (Model Rigaku Multiflex, Tokyo, Japan) was used to identify the crystalline phases. The morphological features of the green tape were observed using a scanning electron microscope (SEM; Model Hitachi S-3500H, Tokyo, Japan).

3. Results and discussion

3.1. Activation energy of crystallization

Crystallization characterization of the GDC powder was estimated from the non-isothermal DSC analysis. Fig. 1 shows the DSC curves of a sample for different heating rates ranging from 10 to 25 °C/min. With increasing heating rate, the exothermic peak shifts to a higher temperature. The crystallization peaks depending on different heating rates can be used

Table 1
Slurry formula of aqueous tape casting GDC.

Additive	Function	Content (wt%)
GDC	Ceramic powder	55
PAA	Dispersant	1
PVA	Binder	5
PEG	Plasticizer	5
Deionized water	Solvent	34

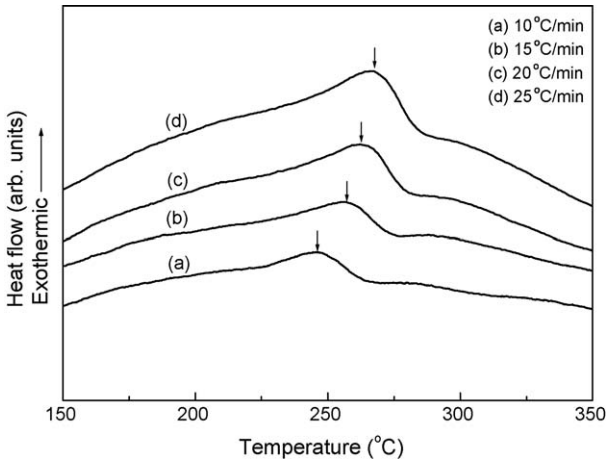

Fig. 1. Differential scanning calorimetry curves of coprecipitation GDC powder at heating rates of 10, 15, 20, and 25 °C/min, respectively.

to estimate the activation energy of crystallization. Through the change in the peak crystallization temperature (T_p) with respect to heating rate, the activation energy of crystallization could be determined using the Kissinger equation as follows [16]:

$$\ln\left(\frac{T_p^2}{\Phi}\right) = \frac{E}{RT_p} + \text{constant} \quad (1)$$

where E is the activation energy of crystallization. T_p is the temperature corresponding to the maximum of the DSC crystallization peak, R is the gas constant (8.314 J/mol), and Φ is the heating rate. The Φs used are 10, 15, 20, and 25 °C/min. If the plot of $\ln(T_p^2/\Phi)$ versus $1/T_p$ is a straight line, and the slope is E/R, the activation energy of the crystallization could be estimated. Fig. 2 shows the Kissinger plot of coprecipitation GDC powder. The activation energy of crystallization is determined using the Kissinger equation to be equal to 88.3 kJ/mol. Moreover, the Avarami exponent n can be determined from the DSC results. The value of the Avrami parameter n, which is a measure of the dimensionality of transformation, is determined using the Ozawa equation [17]:

$$\frac{d\{\ln[-\ln(1-X)]\}}{d\ln\Phi} = -n \quad (2)$$

In this equation, Φ denotes the heating rate, X is the volume fraction crystallized at a specified temperature T, X was determined from the ratio of the partial area crystallized at a certain temperature to the total area of the crystallization exotherm. Here, the total area of the crystallization exotherm ranges between the temperature T_i at which crystallization just begins and the temperature T_f at which crystallization is complete. The partial area crystallized at a certain temperature corresponds to the fraction located between T_i and T [18]. A plot of $\ln[-\ln(1-X)]$ versus $\ln\Phi$ should be a straight line. Then, n can be calculated from the slope of the plot. An n close to 3 indicates bulk or three-dimensional crystal growth and an n value close to 1 indicates surface growth. Intermediate values of n between 1 and 3 indicate that surface and internal crystallizations occur simultaneously [19]. The Ozawa plot of $\ln[-\ln(1-X)]$ versus $\ln\Phi$ is shown in Fig. 3. Here, the volume fraction crystallized was calculated at a specific temperature of 245 °C. n determined from the slope to be 1.17. The result indicates that crystallization is predominated by surface crystallization.

Matusita and Sakka [20,21] proposed that the Kissinger model is valid only when crystal growth occurs on a specific number of nuclei; otherwise, incorrect values for the activation energy are obtained. Therefore, they modified the Kissinger equation to account for nucleation and crystallization growth occurring simultaneously according to

$$\ln\left(\frac{\Phi^n}{T_p^2}\right) = -\frac{mE_c}{RT_p} + \text{constant} \quad (3)$$

where E_c is the activation energy of crystallization and m represents the dimensionality of the crystalline phase. n and m are related through the relation $m = n - 1$. Fig. 4 shows the Matusita and Sakka plot for the determination of the activation

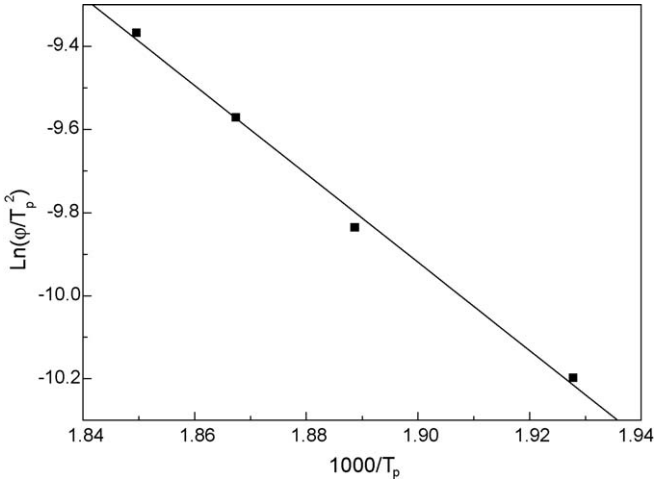

Fig. 2. Plot of $\ln(T_p^2/\Phi)$ against $1/T_p$ for determining the value of crystallization activation energy for GDC.

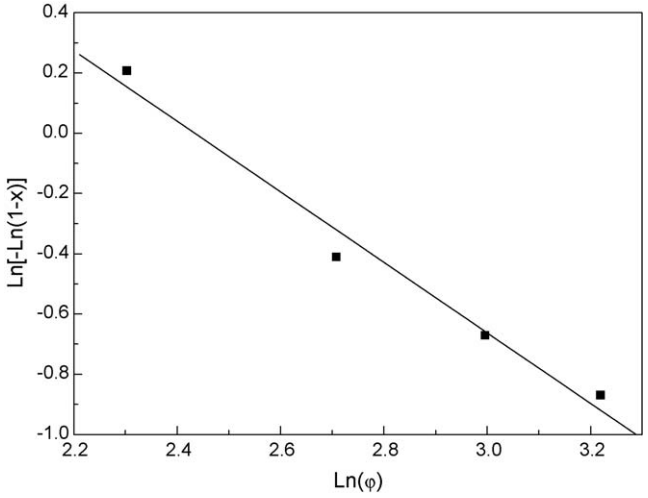

Fig. 3. Plot of $\ln[-\ln(1-X)]$ versus $\ln\Phi$ for determining Avrami constant n.

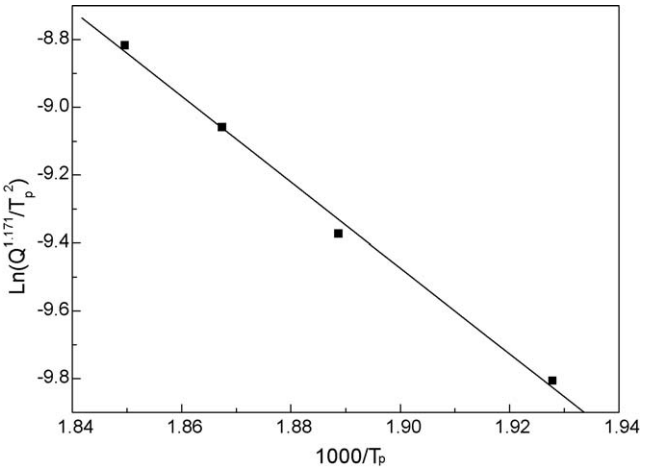

Fig. 4. Plot in accordance with Matusita and Sakka equation for determination of activation energy of crystallization.

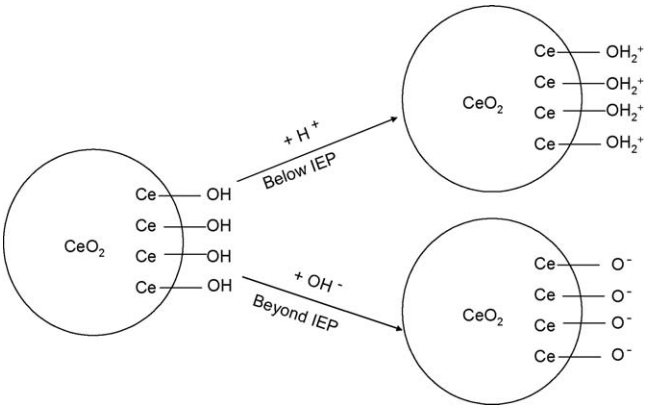

Fig. 6. The production of surface charges on CeO_2 particles by adsorption of ions from acidic or basic solutions.

energy of crystallization, where m is equal to 0.17. By using $n = 1.17$ and $m = 0.17$, and the modified Kissinger equation, we obtained an activation energy of 105.3 kJ/mol.

3.2. Suspension stability

Zeta potential measurements were performed to identify the optimum pH value and dispersant content for GDC suspension as shown in Fig. 5. In the absence of dispersant, the isoelectric point (IEP) was about 4.06. The maximum zeta potential (absolute value) does not exceed 40 mV in the pH range of 2–6, indicating that the electrostatic repulsion between GDC particles is insufficient for stabilizing suspension in the absence of dispersant. For the suspension containing 1.0 wt% PAA dispersant, the zeta potential (absolute value) was about 42 mV at pH = 7. Therefore, we used a content of 1.0 wt% PAA for the tape casting slurry preparation. Noticeably, the dispersant amount is greatly affected the interaction between GDC particles in aqueous suspensions. The function groups of PAA consist of carboxylic acid (COOH) groups, which can exist as COOH or dissociate to COO^-. The dissociation is written as follows:

$$\text{A-COOH} + H_2O \leftrightarrow \text{A-COO}^- + H_3O^+$$

Depending on the pH and ionic strength of the solvent, the fraction of function groups which are dissociated (COO^-) and those which are not dissociated (COOH) will change. Upon increasing the fraction dissociated, the electrical charge on the polymer changes from neutral to highly negative. As the pH increases, the extent of dissociation and negative charge of the polymer increase for PAA. Then as pH increased, a more negative charge adsorbs on the particles surface. It makes the zeta potential move to negative.

According to the literature, metal ions on the surface oxide layer behave as Lewis acids [22]. In presence of water, they may tend to coordinate H_2O molecules. Most oxide surfaces are hydrated and for a metal oxide, there will be MOH groups on the surface [23]. Fig. 6 illustrates the surface charge on CeO_2 particles below or beyond IEP. Below IEP, adsorption of H^+ ions leads a positively charged surface, whereas beyond IEP, adsorption of OH^- ions produces a negatively charged surface. Therefore, in this case, the dissociative chemisorption of water molecules led to an hydroxyl group on surface, which is known to specifically adsorb H^+ and OH^- according to the following equation [13,22]:

$$\equiv\text{Ce}-\text{OH} + H^+ \leftrightarrow \equiv\text{Ce}-\text{OH}_2^+, \quad K_1 = \frac{[\text{Ce}-\text{OH}_2^+]}{[\equiv\text{Ce}-\text{OH}][H^+]} \tag{4}$$

$$\equiv\text{Ce}-\text{OH} + OH^- \leftrightarrow \equiv\text{Ce}-\text{O}^- + H_2O, \quad K_2 = \frac{[\text{Ce}-\text{O}^-]}{[\equiv\text{Ce}-\text{OH}][OH^-]} \tag{5}$$

$$H_2O \leftrightarrow H^+ + OH^-, \quad K_3 = [H^+][OH^-] \tag{6}$$

where K_3 is the equilibrium constant for the dissociation of H_2O, which is referred to as the ionic product of water. At the IEP, $[\text{Ce}–\text{OH}_2^+] = [\text{Ce}–\text{O}^-]$ so that

$$[H^+]_{\text{IEP}} = \left(\frac{K_2K_3}{K_1}\right)^{1/2} \tag{7}$$

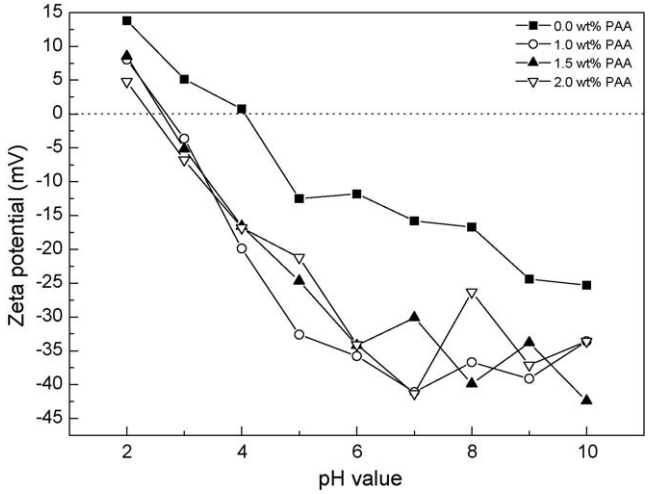

Fig. 5. Zeta potential of GDC powder as a function of pH after addition of various amounts of dispersant.

Since pH is defined as pH = $-\log[H^+]$, the IEP of GDC can be written as:

$$pH_{IEP} = \frac{14+\log K_1-\log K_2}{2} \quad (8)$$

It is obviously, that pH_{IEP} depends on the value of K_1, K_2 and K_3, which are related to the surface chemistry of the powder. With pH_{IEP} = 4.06, are obtained from Eq. (8):

$$\frac{\log K_1-\log K_2}{2} = -2.94 \quad (9)$$

$$\frac{K_1}{K_2} = 10^{-5.88} \quad (10)$$

This indicates that K_2 is much larger than K_1, implying that Eq. (5) dominates the reaction during the chemisorption process. This phenomena can be presumed that the surface $\equiv Ce–OH_2^+$ sites are withdrawn and create $\equiv Ce–O^-$ sites at equilibrium in water. According to the surface properties of CeO_2, polyelectrolyte PAA is selected as dispersant.

3.3. Properties of aqueous tape casting GDC slurries

According to Zeta potential measurements, the dispersant amount of 1 wt% PAA was used for stabilization of slurry containing 55 wt% GDC powder with an adjusted pH of 7. Fig. 7 exhibits viscosity and rheological plots for GDC slurries at 55 wt% loading as a function of shear rate. The results reveal that the viscosity of slurries decrease versus increasing shear rates, typical of ''shear thinning'' behavior. This behavior is due to the attractive interaction of particles and the resultant formation of flocs in the slurry. Shear thinning fluid is preferred in tape casting because it reduces the mobility of constituents in the tape and preserves homogeneity of slurry [24]. The relationship between the viscosity and shear rate can be expressed by the Herschel Bulkley model [25]:

$$\eta = \frac{\tau_Y}{\dot{\gamma}} + K\dot{\gamma}^{\alpha-1} \quad (11)$$

where τ_Y is the yield shear stress necessary to initiate flow, $\dot{\gamma}$ is shear rate, K is the consistency index and n is the shear

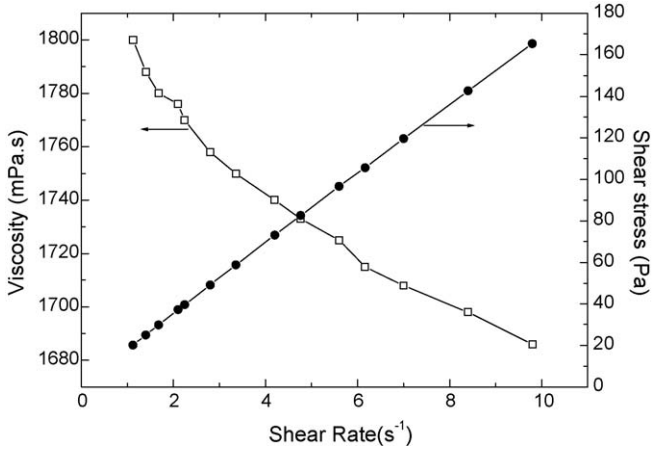

Fig. 7. Rheological and viscosity curves of GDC slurries with 1 wt% PAA as a function of shear rate.

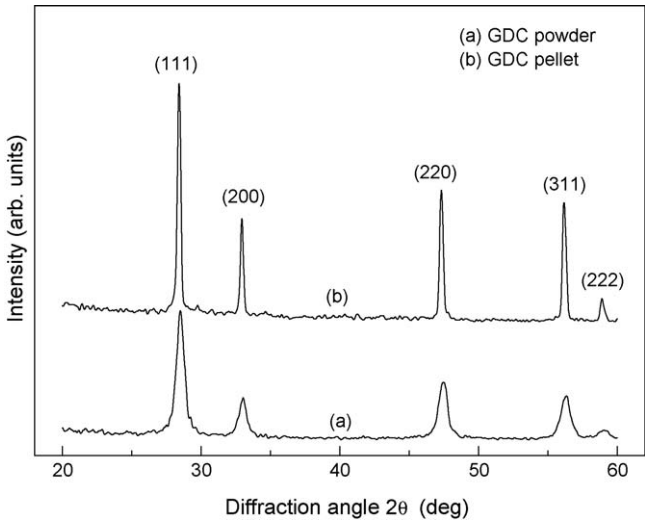

Fig. 8. XRD patterns for (a) GDC powder and (b) GDC sintered at 1500 °C for 5 h.

thinning constant [26]. For a Newtonian behavior, $\alpha = 1$, for a dilatant behavior, $\alpha > 1$, and for *s* pseudoplastic behavior, $\alpha < 1$. Value of τ_Y, K, and α determined according to this equation are 2.321 mPa, 1806.57 mPa, and 0.972, respectively. GDC slurry exhibited pseudoplastic behavior. From experimental results, it is concluded that the optimum composition of slurry was determined as follows: GDC powder 55 wt%, PAA 1 wt%, PVA 5 wt%, PEG 5 wt%, and deionized water 34 wt%.

3.4. Characteristic of green and sintered tapes

Fig. 8(a) reveals the X-ray diffraction patterns of GDC powder after calcinations at 600 °C. Fig. 8(b) shows the X-ray diffraction patterns of the GDC sintered tape after sintered at 1500 °C for 5 h. The figure indicates that GDC powder and sintered tape contain only the cubic fluorite structure with space group *Fm*3*m*, no other crystalline phase is detected. All the peaks in the pattern match well with the Joint Committee of Powder Diffraction Standard (JCPDS) card file no. 34-0394. The crystallite size (D_{XRD}) of GDC powder was calculated according to Scherer equation: $D_{XRD} = 0.9\lambda/(B\cos\theta)$, where λ is the wavelength of the radiation, θ is the diffraction angle, and B is the corrected half-width of the diffraction peak, B is given by $B^2 = B_m^2 - B_s^2$, where B_m is the measured half-width of the diffraction peak and B_s is the half-width of a standard CeO_2 with a crystal size greater than 100 nm. In this study, the reflection from (1 1 1) plane was used to calculate the crystallite size. The result reveals that the crystallite size of GDC powder is 31.2 nm. The microstructure of the green sheet and sintered tape of GDC is shown in Fig. 9, revealing top side of the green tape displays very smooth surface, in which the slurry condition was GDC powder 55 wt%, PAA 1 wt%, PVA 5 wt%, PEG 5 wt%, and deionized water 34 wt%. The homogeneity of the particle packing is ascribed to the fact that the GDC suspensions were well dispersed. In Fig. 9(b), it

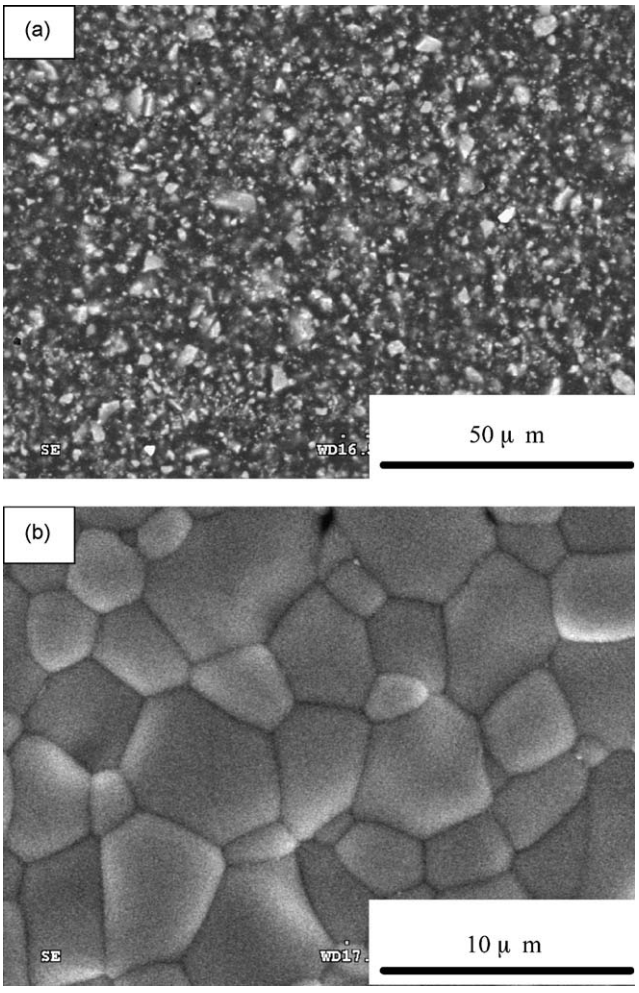

Fig. 9. SEM micrographs of GDC tapes: (a) green tape and (b) sintered tape.

shows good densification, well-sintered, with a grain size ranging from 2 to 5 μm for sintered tape.

4. Conclusions

In this study, using PAA as dispersant, PVA as binder, PEG as plasticizer, and deionized water as solvent, flexible and smooth GDC tapes have been successfully prepared by tape casting process. The isoelectric point for GDC powders in the absence of dispersant was 4.06. In the presence of PAA 1 wt%, PVA 5 wt%, PEG 5 wt%, deionized water 34 wt%, and GDC powders 55 wt% exhibited shear thinning behavior. This indicated that GDC slurry was homogenous and well stabilized. The homogenous particle packing corresponds to the shear thinning behavior of the slurries. Both sides of the green tapes revealed smooth surfaces. No cracks were detected. Moreover, a non-isothermal study of crystallization kinetics of coprecipitated GDC was carried out by DSC measurements. The activation energy of crystallization is determined using the method proposed by Kissinger is equal to 88.3 kJ/mol. The Avrami exponent n related to the dimensionality of crystal growth was determined using the Ozawa equation. In this study, n was equal to 1.17, which indicates that crystallization growth is from surface. By applying the modified Kissinger model, the activation energy of crystallization was found to be 105.3 kJ/mol.

Acknowledgement

The authors would like to thank the National Science Council of Taiwan for financial support of this research under Contract Nos. NSC 96-2221-E-259-005 and NSC 96-2221-E-122-001.

References

[1] B.C.H. Steele, Oxygen transport and exchange in oxide ceramics, J. Power Sources 49 (1994) 1–3.
[2] N.Q. Minh, Ceramic fuel cells, J. Am. Ceram. Soc. 76 (1993) 563–588.
[3] H. Yahiro, Y. Baba, K. Eguchi, H. Arai, High-temperature fuel cell with ceria–yttria solid electrolyte, J. Electrochem. Soc. 135 (1988) 2077–2080.
[4] T. Inoue, T. Setoguchi, K. Eguchi, H. Aria, Study of a solid-oxide fuel cell with a ceria-based solid electrolyte, Solid State Ionics 35 (1989) 285–291.
[5] C.C. Chen, M.M. Nasrallah, H.U. Anderson, Synthesis and characterization of $(CeO_2)_{0.8}(SmO_{1.5})_{0.2}$ thin films for polymeric precursors, J. Electrochem. Soc. 140 (1993) 3555–3560.
[6] H. Yahiro, K. Eguchi, H. Aria, Electrical properties and reproducibilities of ceria–rare-earth oxide systems and their application to solid oxide fuel cell, Solid State Ionics 36 (1989) 71–75.
[7] D.L. Maricle, T.E. Swarr, S. Karavolis, Enhanced ceria—a low temperature SOFC electrolyte, Solid State Ionics 52 (1992) 173–182.
[8] R.N. Blumenthal, F.S. Brugner, J.E. Garnier, The electrical conductivity of CaO-doped nonstoichiometric cerium dioxide from 700 to 1500 °C, J. Electrochem. Soc. 120 (1973) 1230–1237.
[9] J. Cheng, S. Zha, X. Fang, X. Liu, G. Meng, On the green density, sintering behavior and electrical property of tape cast $Ce_{0.9}Gd_{0.1}O_{1.95}$ electrolyte film, Mater. Res. Bull. 37 (2002) 2437–2446.
[10] A. Navarro, J.R. Alcock, R.W. Whatmore, Aqueous colloidal processing and green sheet properties of lead zirconate titanate (PZT) ceramics made by tape casting, J. Eur. Ceram. Soc. 24 (2004) 1073–1076.
[11] L.H. Luo, A.I.Y. Tok, F.Y.C. Boey, Aqueous tape casting of 10 mol%-Gd_2O_3-doped CeO_2 nano-particles, Mater. Sci. Eng. A 429 (2006) 266–271.
[12] T. Chartier, A. Bruneau, Aqueous tape casting of alumina substrates, J. Eur. Ceram. Soc. 12 (1993) 243–247.
[13] J.X. Zhang, D.L. Jiang, S.H. Tan, L.H. Gui, M.L. Ruan, Aqueous processing of titanium carbide green sheets, J. Am. Ceram. Soc. 84 (2001) 2537–2541.
[14] Y. Liu, L. Gao, Effect of 2-phosphonobutane-1,2,4-tricarboxylic acid adsorption on the stability and rheological properties of aqueous nano-sized 3-mol%-yttria-stabilized tetragonal-zirconia polycrystal suspensions, J. Am. Ceram. Soc. 87 (2003) 1106–1113.
[15] J.A. Lewis, Colloidal processing of ceramics, J. Am. Ceram. Soc. 83 (2000) 2341–2359.
[16] H.E. Kissinger, Variation of peak temperature with heating rate in different thermal analysis, J. Res. Natl. Bur. Stand. (U.S.) 57 (1956) 217–221.
[17] T. Ozawa, Kinetic of non-isothermal crystallization, Polymer 12 (1971) 150–158.
[18] C.T. Cheng, M. Lanagan, B. Jones, J.T. Lin, M.J. Pan, Crystallization kinetic and phase development of PbO–BaO–SrO–Nb_2O_5–B_2O_3–SiO_2-based glass-ceramics, J. Am. Ceram. Soc. 88 (2005) 3037–3042.
[19] A.A. Francis, Non-isothermal crystallization kinetics of a blast furnace slag glass, J. Am. Ceram. Soc. 88 (2005) 1859–1863.
[20] K. Matusita, S. Sakka, Kinetics study of crystallization of glasses by differential scanning calorimeter, Phys. Chem. Glasses 20 (1979) 81–84.

[21] K. Matusita, S. Sakka, Kinetics study on crystallization of glass by differential thermal analysis-criterion on application of Kissinger plot, J. Non-Cryst. Solids 38–39 (1980) 741–746.
[22] P.W. Schindler, Surface Complexes at Oxide-Water Interface, Ann Arbor Science Publishers, Ann Arbor, MI, 1981.
[23] M.N. Rahaman, Ceramic Processing and Sintering, Marcel Dekker, Inc., New York, 1995.
[24] X.J. Luo, B.L. Zhang, W.L. Li, H.R. Zhuang, Preparation of aluminum nitride green sheet by aqueous tape casting, Ceram. Int. 30 (2004) 2099–2103.
[25] J.S. Reed, Principles of Ceramics Processing, John Wiley, New York, 1995.
[26] J.H. Feng, F. Dogan, Aqueous processing and mechanical properties of PLZT green tapes, Mater. Sci. Eng. A 283 (2000) 56–64.